# The Effects of Withdrawal Stop Duration in the Directional Solidification of Al-7 wt% Si Alloy on Solidification Parameters, Microstructure, and Microhardness

[1]S. Piseth
[2]D. Masnur

[1]Department of Industrial and Mechanical Engineering, Faculty of Electrical Engineering, Institute of Technology of Cambodia, Russian Federation Boulevard P.O. BOX 86 Phnom Penh, Cambodia

[2]Mechanical Engineering Department, University of Riau, Kampus Bina Widya km 12.5 Simpang Baru, Pekanbaru 28293, Indonesia

Email: [1]pisethseab@gmail.com

**Abstract**
The effects of withdrawal stop duration in the directional solidification of Al-7 wt% Si alloy on solidification parameters, microstructure, and microhardness were investigated. Directional solidification experiments were carried out in five stopping durations: 0 s, 20 s, 30 s, 40 s, and 50 s. Some solidification parameters such as growth rate and temperature gradient were calculated in the stopping region 15 mm from the bottom of the sample. Microstructure parameters such as primary and secondary dendrite arm spacings were defined on both longitudinal and transverse sections in the stopping region, whereas microhardness properties were tested on the longitudinal section in this region. With the rise in the withdrawal stop duration from 0 s to 50 s, the growth rate decreased slightly from 1.26 to 0.84 mm/s, while the temperature gradient remained at 1.71 °C/mm. Furthermore, the microstructure of α-Al dendrites became coarser, and their shapes changed from thin to irregular plates. Primary and secondary dendrite arm spacings increased from 106.4 to 205.7 μm and 19.4 to 38.1 μm, respectively, when the stopping duration was increased. In addition, the hardness decreased from 54.0 to 49.9 HV.

## 1. Introduction

Aluminum-silicon alloys are the most important among cast alloys, and they have widespread applications especially in the aerospace and automotive industries. They exhibit excellent fluidity, castability, corrosion resistance, low specific gravity, high coefficients of thermal expansion, high wear resistance , moderate strength, high ductility, reduced cracking, and improved feeding in the minimization of shrinkage porosity during solidification. Casting in a directional solidification process is critical in the evolution of microstructure. It has been noted that in some applications such as semiconductors, solar cells, heat and fluid flow equipment, the cellular or dendritic microstructure direction affects the efficiency. The best conductibility in heat transfer applications is exhibited in the unidirectional microstructure. Meanwhile, a unidirectional crystal orientation in hypoeutectic Al-Si alloys can be achieved when the alloys contain 5–10 wt% of Si.

Withdrawal rate is the rate of the rod bar in a Bridgman furnace. It is the main parameter affecting the microstructure of a metal alloy during a solidification process. Vibration or change in withdrawal rate affects solidification parameters. To understand the mechanism of solidification, solidification parameters such as temperature gradient (G) and growth rate (V) should be controlled. Meanwhile, microstructure parameters such as primary dendrite arm spacing (PDAS) and secondary dendrite arm spacing (SDAS) determine the mechanical properties of the material. The hardness of the material or alloy depends on the grain size or lamellar spacing: the smaller the lamellar spacing, the higher the hardness.

Thus, in the present work, an attempt was made to investigate the effects of withdrawal stop duration in the directional solidification of Al-7 wt% Si alloy on solidification parameters, microstructure, and microhardness. We will also briefly discuss the relationships between growth rate, dendrite arm spacing (DAS), and microhardness.

## 2. Materials and Methods

### 2.1. Materials

High-purity Al (99.95 wt%) and Al-15 wt% Si master alloy were weighted and melted in an electric furnace to prepare a new master alloy composition with 7 wt% Si. The raw materials and samples were analyzed by Thermo Scientific™ ARL iSpark™ OES to ensure their chemical composition. The chemical composition of the alloy is shown in Table 1.

Table 1. Chemical Composition of the Samples

| Element | Al | Si | Fe | Other |
|---------|-------|------|------|--------|
| wt. % | 92.54 | 7.00 | 0.32 | ±0.01 |

### 2.2. Directional Solidification Method

The directional solidification of the sample alloy was performed in a Bridgman-type directional solidification furnace. The experimental apparatus is schematically shown in Figure 1. The detail of the Bridgman-type furnace is shown in Figure 2. Using the Bridgman method, molten alloy was poured into a clay mold (60 mm in length, 6 mm in internal diameter, and 10 mm in external diameter). There were six holes along the mold into which K-type thermocouples were inserted to measure the temperatures during melting and freezing. The thermocouples were mounted at $T_1$ = 5 mm, $T_2$ = 15 mm, $T_3$ = 25 mm, $T_4$ = 35 mm, $T_5$ = 45 mm, and $T_6$ = 55 mm from the bottom of the clay mold (see in Figure 3a). The temperature data were recorded by a data-logger and transferred to a computer (see in Figure 1).

The samples making was through two processes. Firstly, the aluminum-silicon alloy was melted in the electric furnace at 700 ˚C. The molten alloy was poured into a permanent mold (PM) to fabricate cylindrical samples with dimensions of 6 mm in diameter and 60 mm in length. Before the pouring, the carbon steel mold was pre-heated to around 150 ˚C. A resulting PM sample is shown in Figure 3b. Secondly, The PM samples were re-melted in the Bridgman-type solidification

apparatus. To ensure that the temperature in the furnace was uniform, the temperature of 700 °C at which the samples were melted was held for around 30 minutes. In this process, the samples were pulled down by a synchronous motor at a constant withdrawal rate of 16.433 μm/s. The samples were quenched for 35 s at a constant flow rate during the downward movement, and then the motor was stopped for durations of 0 s, 20 s, 30 s, 40 s, and 50 s. Past each of the stopping durations above, the motor was moved downward again until outsize of furnace. One of the products of the directional solidification is shown in Figure 3c.



Figure 3. Sample and mold: (a) clay mold; (b) PM sample; (c) directional solidification sample

### 2.3. Calculation of Solidification Parameters

Solidification parameters such as temperature gradient and growth rate were calculated based on temperature, solidification time, and thermocouple distance between $T_2$ and $T_5$. Those positions were selected based on the estimation of the region of dendrites growth between the minimum and the maximum during the withdrawal stop duration. The thermocouple distances are shown in Figure 3a. $T_2$ is the temperature of the second thermocouple at the solid-liquid interface, $T_5$ is the temperature of the fifth thermocouple in a liquid phase, and $\Delta T$ is the temperature difference between $T_2$ and $T_5$. The thermocouple distance from $X_2$ to $X_5$ is $\Delta X$. Temperature gradient is defined by the ratio of $\Delta T$ to $\Delta X$ ($G=\Delta T/\Delta X$), whereas growth rate (V) is calculated by the formula $V=\Delta X/\Delta t$. $\Delta t$ is the time taken to reach the solid-liquid interface from $T_2$ to $T_5$ [11]–[13].

### 2.4. Microstructure Observation

The quenched samples were cut along the longitudinal and transverse axes. Those sections were cold-mounted with epoxy-resin and then mechanically wet-ground with SiC paper to 5,000 grit. After
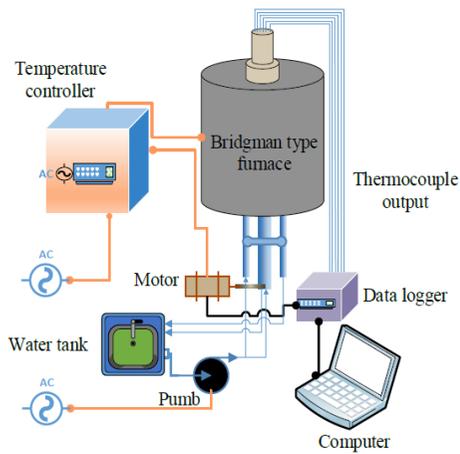


Figure 1. Bridgman-type directional solidification experimental system and equipment
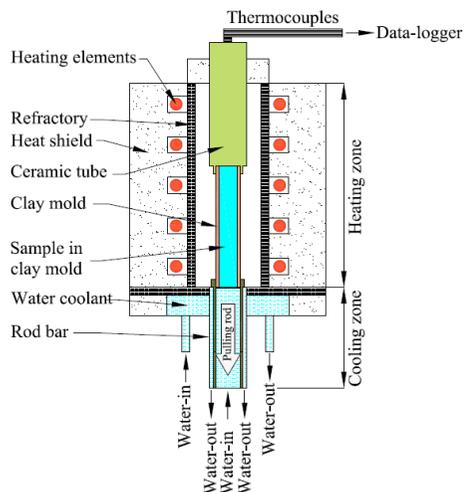


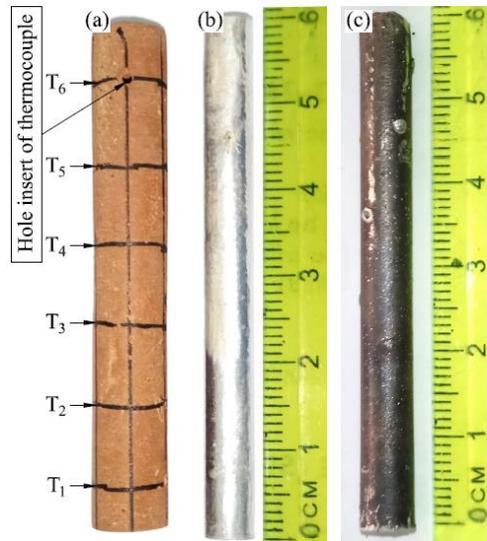Figure 2. Details of Bridgman-type directional solidification furnace

polishing, those sections were etched with NaOH solution for 2–3 s (95 ml $H_2O$ and 10 g NaOH) for metallographic observation.

The microstructure in both longitudinal and transverse sections was photographed with an Olympus C-35AD-4 microscope camera bottom up at the same magnification.

### 2.5. Measurement of Microstructure Parameters

PDAS and SDAS were measured in the stopping region using the ImageJ 1.52i software [14]. In this section, the simple method was used to calculate the SDAS [15] using the formula $SDAS = L/(n-1)$, where $L$ is dendrite length and $n$ is the total number of secondary dendrites.

### 2.6. Microhardness Testing

The hardness of the samples on the longitudinal section was monitored by the Boehler Vickers hardness testing machine. The monitoring was carried out with a load of 50 g and a loading duration of 10 s. The samples were evaluated in the stopping region 15 to 50 mm from the bottom.

### 3. Results and Discussions

### 3.1. The Effects of Withdrawal Stop Duration on Solidification Parameters

Figure 4 shows the growth rates which varied with stopping duration, and Figure 5 the temperature gradient values which varied with stopping duration. The growth rate fell slightly from 1.26 to 0.84 mm/s when the stopping duration was increased from 0 s to 50 s. On the other hand, the average values of temperature gradient in various stopping durations were highly similar (see in Figure 5). The maximum value was 1.82 ˚C/mm, achieved in the stopping duration of 20 s, and the minimum value was 1.61 ˚C/mm, achieved in the stopping duration of 0 s. The temperature gradient values were not significantly different. Thus, it can be assumed that the temperature gradient was constant. Throughout the stopping durations of 0 s to 50 s in the directional

solidification process, the temperature gradient did not change significantly, with an average value of 1.71 ˚C/mm. According to these results, the temperature difference between $T_2$ and $T_5$ was very small despite the stopping duration increase. The rod bar in the Bridgman-type furnace pulled the samples downward during the process from the heating to the cooling zones. In this situation, the sample of a longer withdrawal stop duration had a slower growth rate than that of a shorter one. These results show that withdrawal stop duration would affect other parameters such as microstructure, DAS, and hardness.
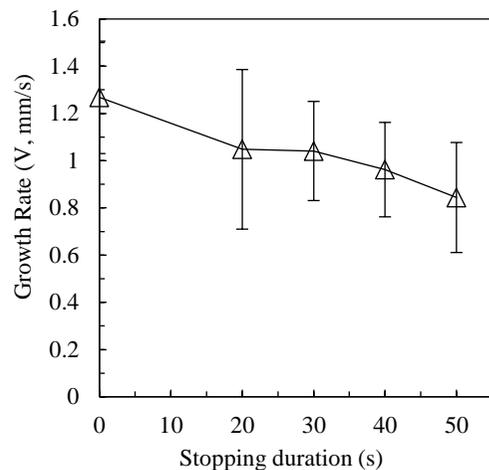


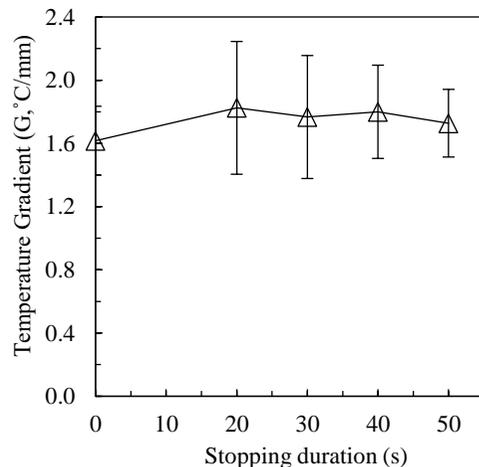Figure 4. Relationship between growth rate and stopping duration



Figure 5. Relationship between temperature gradient and stopping duration

### 3.2. Effects of Withdrawal Stop Duration on Microstructure

Figure 6a-e shows the microstructure of the columnar dendrites and the directionally solidified DAS on the longitudinal section in different stopping durations. The microstructure on the transverse section in each stopping duration is shown in Figure 7a-e. The results show that α-Al dendrites became coarser and that their shapes changed from thin to round or oval when the stopping duration was increased. As can be seen in Figure 6a, the PDAS was very close and the SDAS was fine. In contrast, the SDAS was wide when the withdrawal stop duration of 50 s was applied (see in Figure 6e). In addition, the equiaxed columnar dendrites on the transverse section grew longer when the stopping duration rose (see in Figure 7). Withdrawal stop duration decelerated the solute growth, allowing diffusion in the liquid, which in turn tended to enlarge the SDAS. The SDAS was controlled by a coarsening process. Under this condition, some dendrites disappeared or merged together, resulting in increases in the spacing between arms. This promoted growth of dendrite branches. This is the main mechanism to promote α-Al dendrites coarseness. Furthermore, the different sizes of dendrites were linked to growth rate and cooling rate. Higher growth and cooling rates provided smaller dendrite arms. Thus, stopping duration influenced the solute-rich liquid distribution and in turn the microstructure.

### 3.3. Effects of Withdrawal Stop Duration on Microstructure Parameters

Figure 8 shows variations of PDAS and SDAS with stopping duration. The results showed that DAS and SDAS increased dramatically from 106.4 to 205.7 μm and 19.4 to 38.1 μm, respectively, when the stopping duration rose from 0 s to 50 s. Several factors affecting PDAS and SDAS were temperature gradient, growth rate, and cooling rate. Dendrite transformation was linked to temperature gradient and growth rate . PDAS appeared to be linked to solidification parameters, and SDAS was controlled by solidification time. Withdrawal stop duration allowed for freezing time, causing the growth rate to be slow. As documented in, while the temperature gradient increased, the growth rate remained constant. Under this condition, the PDAS and SDAS values became reduced. In contrast, while the growth rate increased, the temperature gradient remained constant. The PDAS and SDAS values decreased. According to the results of the present work, both PDAS and SDAS increased when the growth rate decreased, whereas the temperature gradient remained constant. Thus, the present work is in agreement with the previous report.
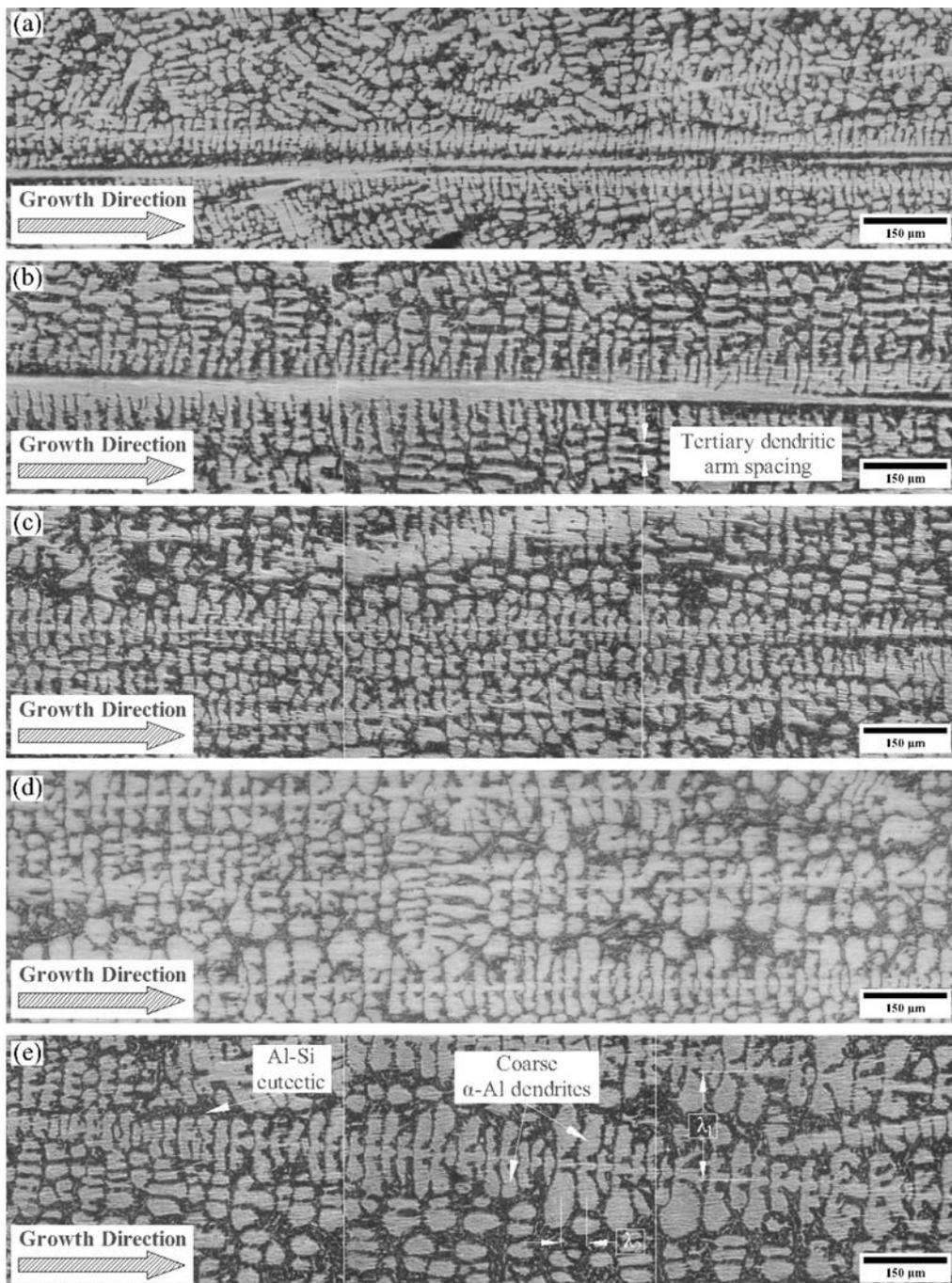
Figure 6. Microstructure on the longitudinal section in stopping durations: (a) 0 s; (b) 20 s; (c) 30 s; (d) 40 s; and (e) 50 s
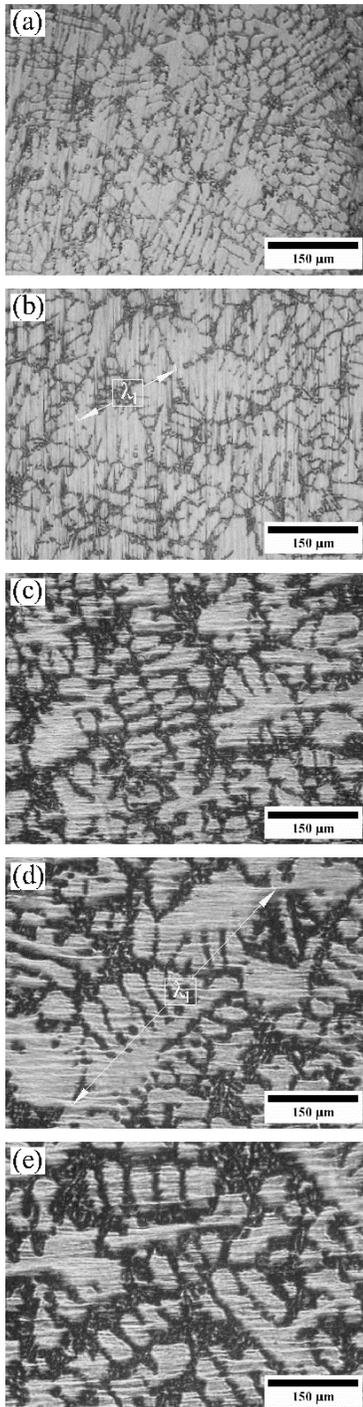
Figure 7. Microstructure on the transverse section in stopping durations: (a) 0 s; (b) 20 s; (c) 30 s; (d) 40 s; and (e) 50 s
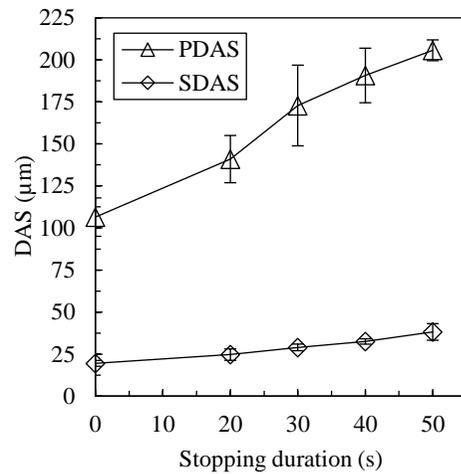


Figure 8. Relationship of PDAS and SDAS to stopping duration

### 3.4. **Effects of Withdrawal Duration on Microhardness**

Variation of microhardness values with stopping duration is shown in Figure 9. According to the results, microhardness decreased slightly when the withdrawal stop duration increased. When the stopping duration was extended from 0 s to 50 s, the hardness value was reduced from 54.0 to 49.9 HV. In general, microhardness depends on microstructure features like lamellar spacing or grain size: the finer the DAS, the better the mechanical properties, or the smaller the laminar spacing, the higher the hardness. Larger grain or dendrite sizes provide lower bonding forces between atoms because of easier atoms dislocation. This means that smaller grains or dendrite arms have greater ratios of surface area to volume and lead to greater obstacles to dislocation.
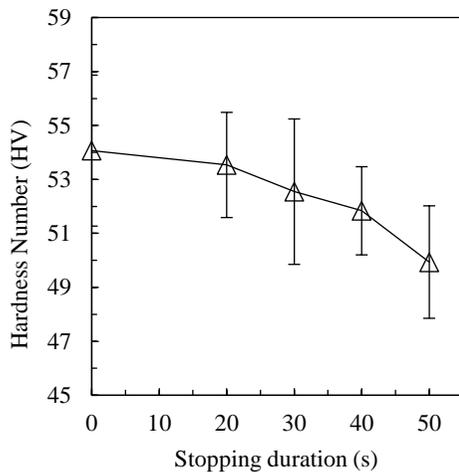
Figure 9. Variation of hardness value with stopping duration

### 3.5. Relationships between Growth Rate, Microhardness, and Dendrite Arm Spacing

Figure 10 shows the relationship between DAS and hardness, Figure 11 shows the relationship between growth rate and hardness, and Figure 12 .shows the relationship between growth rate and DAS. Those figures were obtained when the withdrawal stop duration was varied from 0 s to 50 s at constant temperature gradient of 1.74 °C/mm. As can be seen in Figure 10, hardness fell slightly when DAS increased. The highest hardness value of 54.0 HV was achieved when the PDAS achieved a minimum of 106.4 μm and SDAS achieved a minimum of 19.4 μm. Furthermore, hardness increased with the increase in growth rate (see in Figure 11). In addition, while the growth rate raised, the DAS declined steeply. The smallest values of PDAS and SDAS were found at the maximum growth rate of 1.26 mm/s (see in Figure 12). On the other hand, the largest PDAS value of 205.7 μm and the largest SDAS value of 38.1 μm where obtained when the growth rate was at its minimum (0.84 mm/s). Thus, mechanical properties can be improved by making the DAS finer. As reported in and increases in solidification parameters led to increases in microhardness. Not only hardness but also ultimate strength, ductility, and elongation fell when DAS

increased. It was revealed that microstructure varied with growth rate. If the growth rate was high, the microstructure became finer. Moreover, microstructure failed to achieve accuracy uni-directionally if dendrites grew fast.
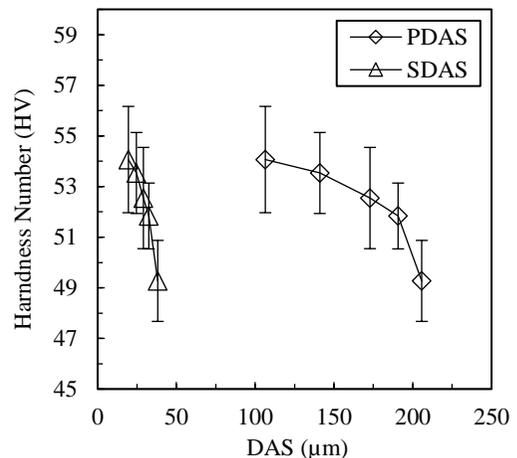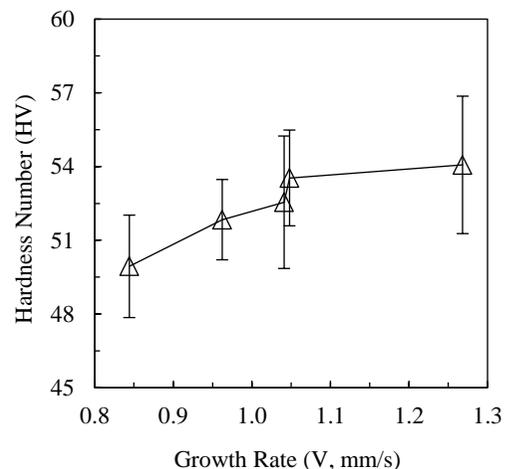


Figure 10. Relationship between hardness and DAS



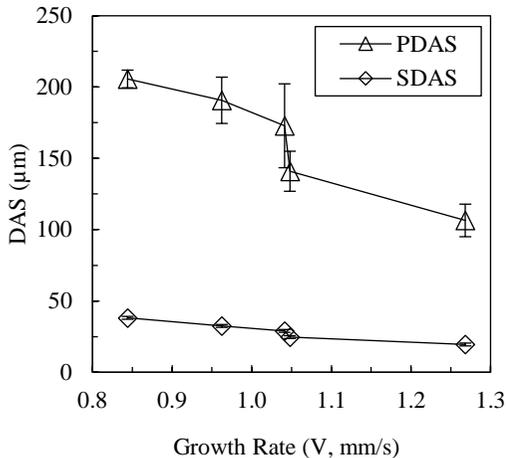Figure 11. Relationship between growth rate and hardness

Figure 12. Relationship between growth rate and DAS

## 4. Conclusion

In this work, we experimentally examined the effects of withdrawal stop duration in the directional solidification of Al-7 wt% Si alloy on solidification parameters, microstructure, and microhardness. The following conclusions can be drawn from the experimental results. When the withdrawal stop duration was extended from 0 s to 50 s:

- the solidification parameter growth rate decreased slightly from 1.26 to 0.84 mm/s, while the solidification parameter temperature gradient was constant at 1.71 °C/mm,
- the microstructures of α-Al dendrites became coarser, and their shapes changed from thin to irregular plates; the values of primary and secondary dendrite arm spacings increased from 106.4 to 205.7 μm and 19.4 to 38.1 μm, respectively, and
- the microhardness value decreased from 54.0 to 49.9 HV.

## 5. Acknowledgments

## 6. References

D. M. Stefanescu, Science and engineering of casting solidification, Third Edit. SpringerInternational Publishing Switzerland 2015, 2009.

F. C. Robles-Hernandez, J. M. H. Ramírez, and R. Mackay, Al-Si Alloys. 2017.

H. Kaya and A. Aker, "Effect of alloying elements and growth rates on microstruture and mechanical properties in the directionally solidified Al-Si-X alloys," J. Alloys Compd., vol. 694, pp. 145–154, 2017.

H. Kaya, E. Çadirli, and M. Gündüz, "Dendritic growth in an aluminum-silicon alloy," J. Mater. Eng. Perform., vol. 16, no. 1, pp. 12–21, 2007.

H. Kaya, E. Çadirli, M. Gündüz, and A. Ülgen, "Effect of the temperature gradient, growth rate, and the interflake spacing on the microhardness in the directionally solidified Al-Si eutectic alloy," J. Mater. Eng. Perform., vol. 12, no. 5, pp. 544–551, 2003.

H. Zhong et al., "Effect of interdendritic thermoelectric magnetic convection on evolution of tertiary dendrite during directional solidification," J. Cryst. Growth, vol. 439, pp. 66–73, 2016.

J. Campbell, Complete Casting, First edit. Elsevier, 2011.

J. G. Kaufman and E. L. Rooy, Aluminum Alloy Castings: Properties , Processes , and Applications. 2004.

J. R. Davis, "Aluminum and Aluminum Alloys," in ASM International, 2001, pp. 351–416.

K. G. Basavakumar, P. G. Mukunda, and M. Chakraborty, "Influence of grain refinement and modification on microstructure and mechanical properties of Al-7Si and Al-7Si-2.5Cu cast alloys," Mater. Charact., vol. 59, no. 3, pp. 283–289, 2008.

M. Gupta and S. Ling, "Microstructure and mechanical properties of hypo/hyper-eutectic Al-Si alloys synthesized using a near-net shape forming technique," J.

Alloys Compd., vol. 287, no. 1–2, pp. 284–294, 1999.

M. Okayasu and S. Takeuchi, "Crystallization characteristics of cast aluminum alloys during a unidirectional solidification process," Mater. Sci. Eng. A, vol. 633, pp. 112–120, 2015.

M. Şahin and E. Çadirli, "The effects of temperature gradient and growth rate on the microstructure of directionally solidified Sn-3.5Ag eutectic solder," J. Mater. Sci. Mater. Electron., vol. 23, no. 2, pp. 484–492, 2012.

N. Maraşli, K. Keşlioğlu, B. Arslan, H. Kaya, and E. Çadirli, "Effects of growth rate and temperature gradient on the microstructure parameters in the directionally solidified succinonitrile-7.5 wt.% carbon tetrabromide alloy," J. Mater. Process. Technol., vol. 202, no. 1–3, pp. 145–155, 2008.

S. Engin, U. Büyük, and N. Maraşli, "The effects of microstructure and growth rate on microhardness, tensile strength, and electrical resistivity for directionally solidified Al-Ni-Fe alloys," J. Alloys Compd., vol. 660, pp. 23–31, 2016.

S. Steinbach and L. Ratke, "The influence of fluid flow on the microstructure of directionally solidified AlSi-base alloys," Metall. Mater. Trans. A, vol. 38 A, no. 7, pp. 1388–1394, 2007.

U. Böyük, S. Engin, and N. Maraşli, "Microstructural characterization of unidirectional solidified eutectic Al-Si-Ni alloy," Mater. Charact., vol. 62, no. 9, pp. 844–851, 2011.

W. Rasband, "Downloads - ImageJ," 2018. [Online]. Available: https://imagej.net/Downloads. [Accessed: 12-Apr-2019].

Y. Kaygısız and N. Maraşlı, "Directional solidification of Al–Cu–Si–Mg quaternary eutectic alloy," J. Alloys Compd., vol. 721, pp. 764–771, 2017.

Y. Koçak, S. Engin, U. Böyük, and N. Maraşlı, "The influence of the growth rate on the eutectic spacings, undercoolings and microhardness of directional solidified bismuth–lead eutectic alloy," Curr. Appl. Phys., vol. 13, no. 3, pp. 587–593, 2013.